Electronic Supplementary Material (ESI) for Physical Chemistry Chemical Physics.

Supporting information for:

Mechanisms and Dynamics of Protonation and Lithiation of Ferrocene

Nishant Sharma, Jayanth K. Ajay, Krishnan Venkatasubbaiah, and Upakarasamy Lourderaj*

School of Chemical Sciences, National Institute of Science Education and Research, Bhubaneswar, Odisha, INDIA

E-mail: u.lourderaj@niser.ac.in

*To whom correspondence should be addressed

Computational Details

The potential energy profiles for protonated and lithiated ferrocene were mapped using B3LYP[S1,S2] and BPW91[S3,S4] functionals and DZVP[S5,S6] basis set. The stationary point structures were characterized by computing harmonic vibrational frequencies. GAUSSIAN 09[S7] and NWChem[S8] software were used to carry out these calculations. The protonation and lithiation energies were found to be 211.06 and 41.52 kcal/mol respectively. All the energies reported here are without zero-point-energy correction. At BPW91/DZVP level, **MP** and **AG** were found to be nearly degenerate. B3LYP/DZVP results were closer to CCSD(T)/pVDZ[S9] ones and hence the ab initio trajectories were calculated using this level of theory.

Ab initio classical trajectories[S10,S11] were performed to understand the unimolecular as well as the bimolecular dynamics of protonation and lithiation of ferrocene using VENUS/NWChem,[S12] where the ab initio forces were computed at B3LYP/DZVP level of theory. The initial coordinates and momenta were selected using quasi-classical sampling procedure.[S13] The trajectories were integrated numerically using velocity-Verlet algorithm,[S14] using a time step of 0.5 fs in protonation reaction, and 0.5 fs and 0.3 fs for unimolecular and bimolecular dynamics in lithiation reaction. The trajectories were numerically integrated for 0.5-1 ps. The typical CPU time for $\sim$1 ps integration of a trajectory on a 8 core Intel Xeon (3.0 GHz) processor is $\sim$6 days.

In unimolecular dynamics study of protonated ferrocene, the trajectories were initiated from **MP** and **AG** minima, and the initial coordinates and momenta were chosen using a Boltzmann distribution of vibrational and rotational energies at 300 K. For bimolecular collision dynamics, the trajectories were initiated with ferrocene and H^+ separated by 8 Å and with Boltzmann distribution of vibrational and rotational energies for ferrocene at 300 K. However, these trajectories failed due to SCF convergence issues at large separation between ferrocene and H^+ during initialization. To overcome the problem and mimick bimolecular collisions, trajectories were initiated using three partially optimized structures (Fig. S4) obtained by fixing (i) the endo C-H distance at 5 Å in **AG**, (ii) H^+ on top of the Cp ring with $\angle X_1$-Fe-H = 4.6° and Fe-H at 6.6 Å (iii) $\angle X_1$-Fe-H at 41.8° and Fe-H at 7.48 Å. The three optimized structures had one imaginary frequency and are 105.4,

97.9, and 98.0 kcal/mol above **AG** in energy. A Boltzmann distribution of energies is assumed at these structures. A total of 182 trajectories were initiated with different orientations of H^+ about ferrocene with Boltzmann distribution of vibrational and rotational energies at 300 K. Of the 182 trajectories, 80 resulted in the protonation of ferrocene. In the remaining 102 trajectories, H^+ moved away from ferrocene, and these trajectories were terminated after 200 fs.

The unimolecular dynamics study of lithiated ferrocene was performed by following trajectories initiated at **TSe** and **TSf**. For bimolecular collision reaction, trajectories were initiated with ferrocene and Li^+ separated by 8 Å and relative kinetic energy of 0.89 kcal/mol corresponding to 300 K. The impact parameter (b) was taken to be zero for effective collisions. 80 trajectories were integrated, and all of them resulted in lithiation of ferrocene. Additional trajectories were calculated for $b = 2$ and $b = 5$ Å (8 each), and all of them were reactive.

Table S1: Comparison of structural parameters and relative energies of ferrocene and its protonated forms.

	MP			**AG**			**Ferrocene**		
	BPW91[a]	B3LYP[a]	B3LYP[b]	BPW91[a]	B3LYP[a]	B3LYP[b]	BPW91[a]	B3LYP[a]	B3LYP[b]
Fe-H^+(Å)	1.50	1.48	1.49	1.58	1.67	1.70	-	-	-
C-H^+(Å)	1.87	1.87	1.88	1.36	1.23	1.22	-	-	-
Fe-X_1(Å)[c]	1.68	1.71	1.70	1.67	1.71	1.70	1.64	1.68	1.67
Fe-X_2(Å)[d]	1.68	1.71	1.70	1.68	1.70	1.69	1.64	1.68	1.67
X_1-Fe-X_2 (°)	167	167	167	169	169	169	180	180	180
X_1-Fe-H^+ (°)	97	97	97	80	74	74	-	-	-
C-H (Å)	-	-	-	-	-	-	1.09	1.08	1.08
Fe-C (Å)	-	-	-	-	-	-	2.05	2.08	2.07
Structure	eclipsed	eclipsed	eclipsed	eclipsed	eclipsed	eclipsed	eclipsed	eclipsed	eclipsed
ΔE [e] (kcal/mol)	-0.03	2.60	2.58	0	0	0	-	-	-

[a]6-311++G** basis set. [b]DZVP basis set. [c]X_1 is the center of the Cp ring which is closer to the H^+. [d]X_2 is the center of the Cp ring which is farther from the H^+. [e]$\Delta E = E_{\mathbf{MP}} - E_{\mathbf{AG}}$ at different levels of theory .

Table S2: Comparison of structural parameters and relative energies of three different transition states.

	TSb			**TSa**			**TSd**			**TSc**[c]
	BPW91[a]	B3LYP[a]	B3LYP[b]	BPW91[a]	B3LYP[a]	B3LYP[b]	BPW91[a]	B3LYP[a]	B3LYP[b]	B3LYP[b]
Im. Freq (cm^{-1})	44i	29i	30i	290i	144i	308i	653i	742i	848i	48i
Fe-H^+(Å)	1.59	1.68	1.71	1.52	1.48	1.50	-	-	-	1.48
C-H^+(Å)	1.34	1.22	1.21	1.57	1.80	1.70	1.29	1.28	1.29	1.91
Fe-X_1(Å)[d]	1.67	1.71	1.70	1.67	1.70	1.69	1.59	1.64	1.62	1.71
Fe-X_2(Å)[e]	1.68	1.71	1.69	1.68	1.71	1.70	1.67	1.70	1.68	1.70
X_1-Fe-X_2 (°)	168	169	169	168	167	167	178	178	178	159
X_1-Fe-H^+ (°)	79	74	74	87	94	91	25	25	25	98
Structure	staggered	staggered	staggered	eclipsed	eclipsed	eclipsed	eclipsed	eclipsed	eclipsed	staggered
ΔE [f] (kcal/mol)	0.85	0.37	0.31	0.13	2.60	2.63	20.1	20.09	20.29	5.16

[a]6-311++G** basis set. [b]DZVP basis set. [c]**TSc** could not be located for B3LYP/6-311++g** and BPW91/6-311++g** levels of theory. [d]X_1 is the center of the Cp ring which is closer to the H^+. [e]X_2 is the center of the Cp ring which is farther from the H^+. [f]Energies relative to **AG** at different levels of theory.

Table S3: Comparison of structural parameters and relative energies of lithiated ferrocene using B3LYP/DZVP level of theory.

	CP	TSe	ML	TSf
Fe-Li(Å)	3.60	3.53	2.46	2.53
C-Li(Å)	2.32	2.23	2.49	2.34
Li-H(Å)	3.06	1.97	2.49	2.19
Fe-X_1(Å)[a]	1.64	1.68	1.69	1.70
Fe-X_2(Å)[b]	1.68	1.67	1.69	1.70
C-X_1-Fe-Li(°)	-	-	44.15	4.01
X_1-Fe-Li(°)	0.06	61.33	94	95.23
Structure	eclipsed	eclipsed	eclipsed	eclipsed
ΔE^c (kcal/mol)	0	23.62	7.05	8.52

[a] X_1 is the center of the Cp ring which is closer to the Li^+. [b] X_2 is the center of the Cp ring which is farther from the Li^+. [c] Energies are given relative to **CP**.

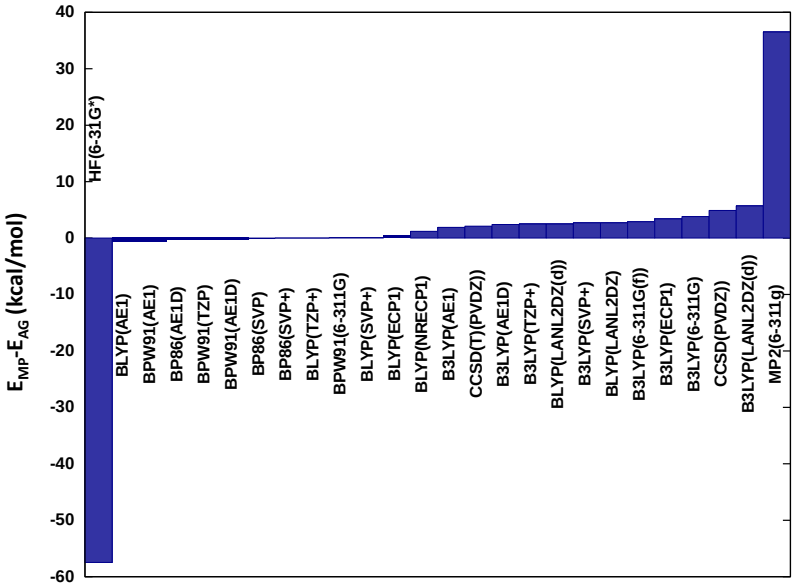

Fig. S1: Comparison of energy differences between metal-protonated (**MP**) and agostic (**AG**) structures in different levels of theory.

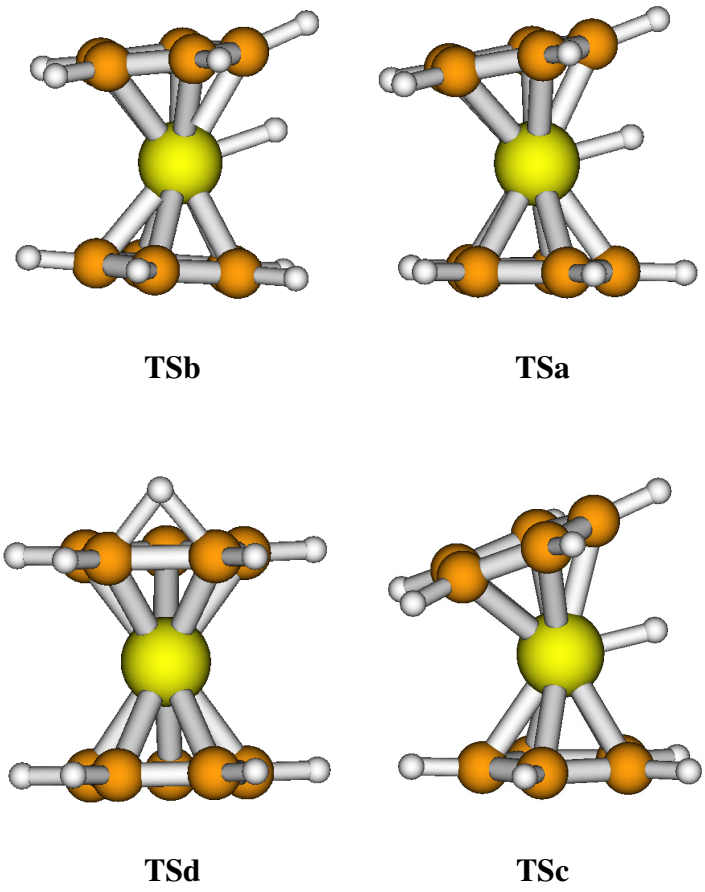

(a)

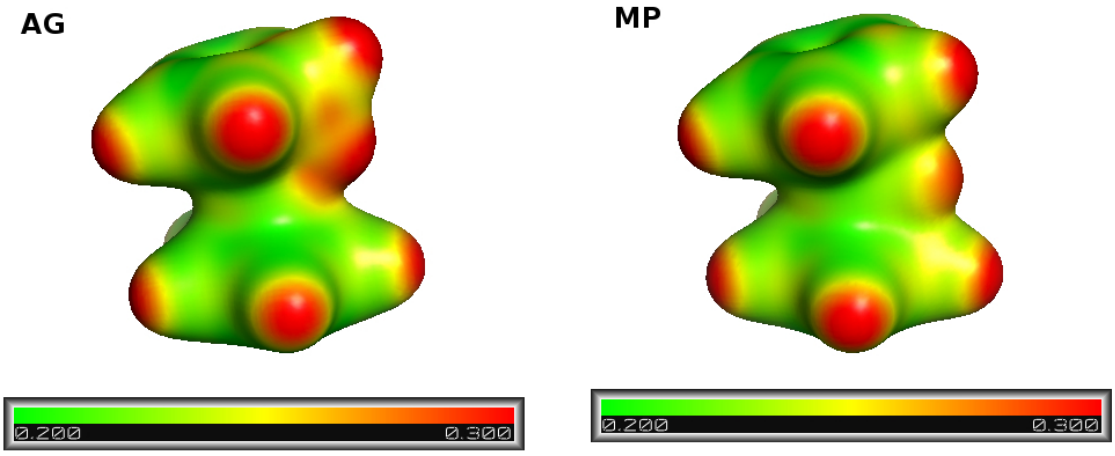

(b)

Fig. S2: (a) Structures of **TSb**, **TSa**, **TSd** and **TSc** of protonated ferrocene. (b) MEP (in a.u.) map for **AG** and **MP** of protonated ferrocene

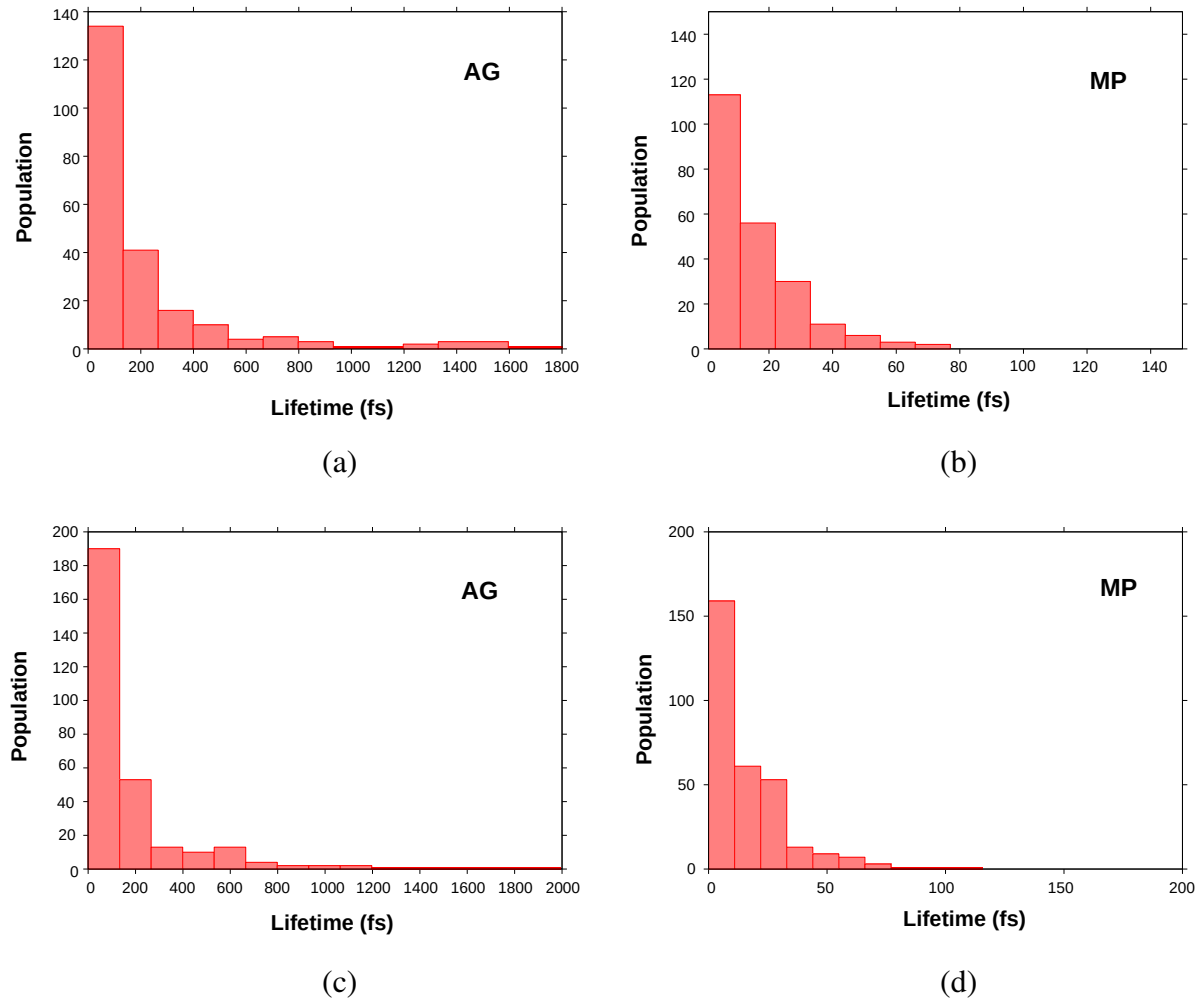

Fig. S3: Plot of population vs lifetime for agostic and metal-protonated forms when the trajectories were initiated from **AG** (a and b) and **MP** (c and d) minima respectively.

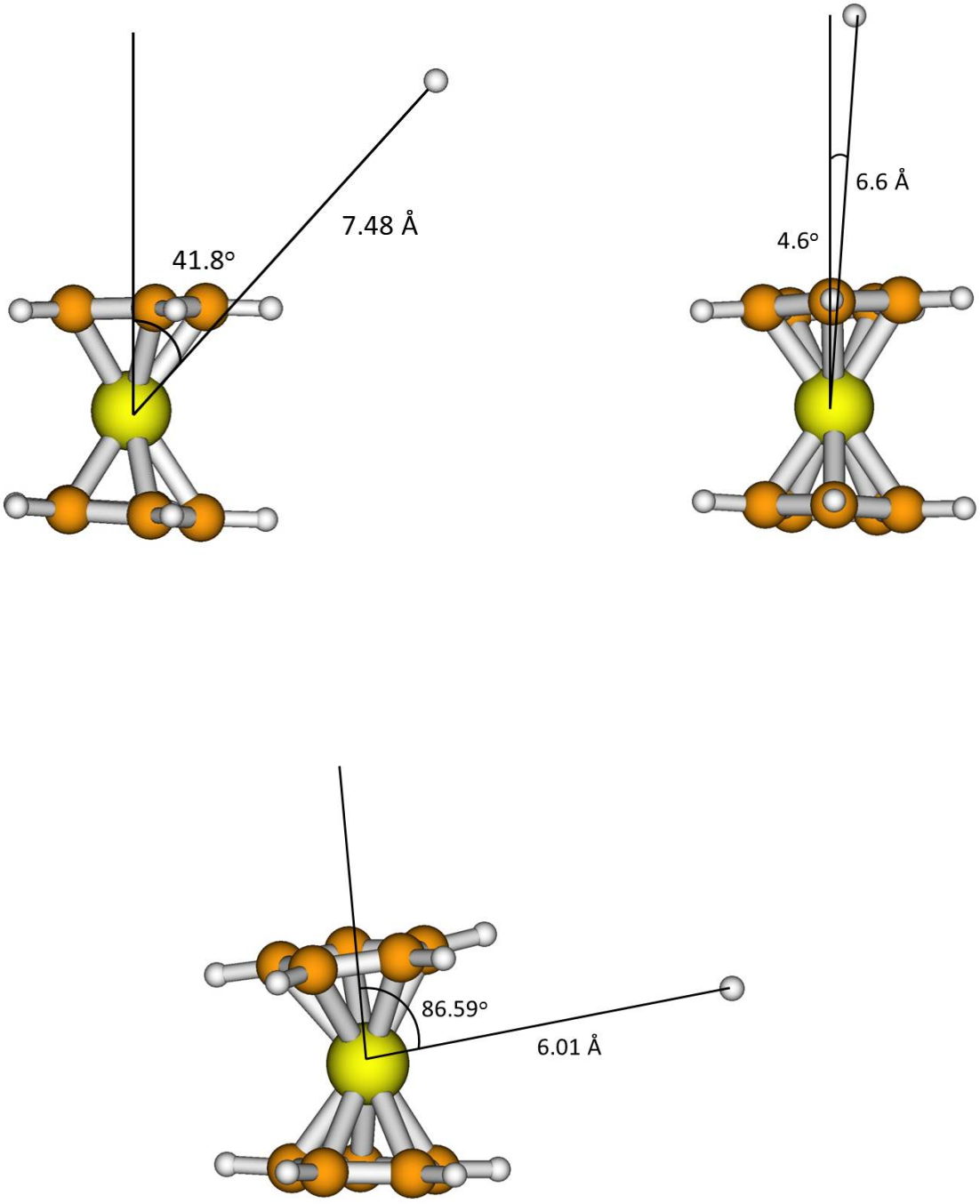

Fig. S4: Geometries used to sample trajectories for protonation of ferrocene to represent bimolecular collision.

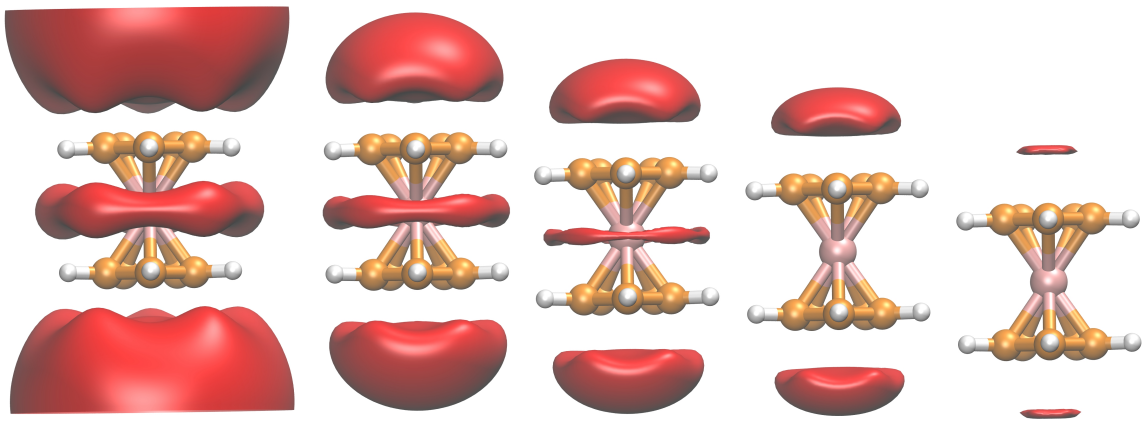

(-0.003) (-0.013) (-0.018) (-0.022) (-0.03)

Fig. S5: Electrostatic potential (in a.u.) map of ferrocene for different iso-values.

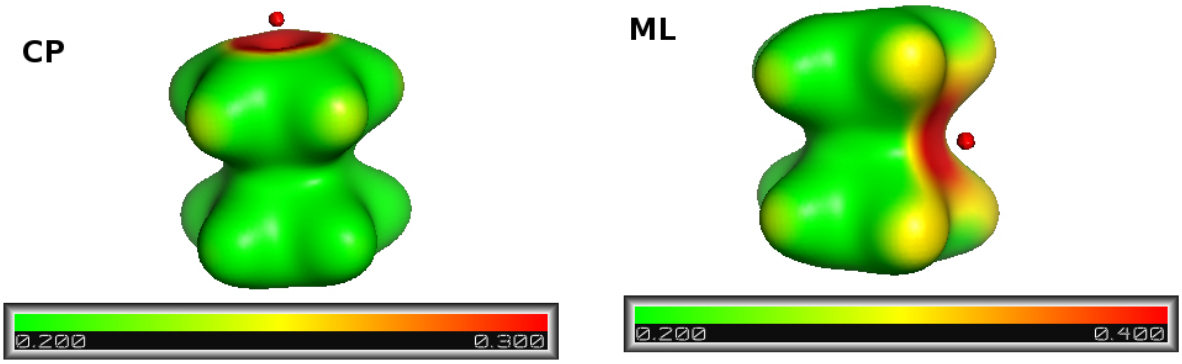

Fig. S6: MEP (in a.u.) map for **CP** and **ML** of lithiated ferrocene.

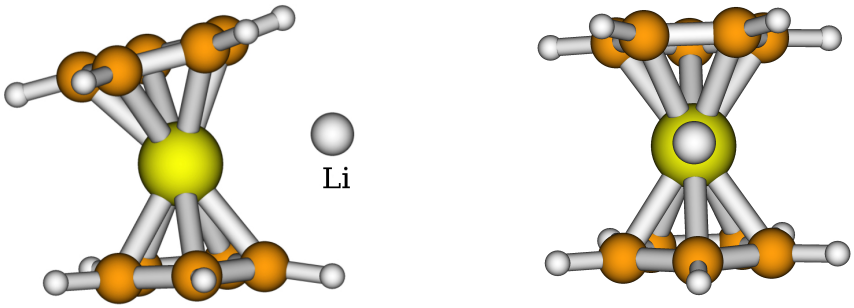

(Side view) (Front view)

Fig. S7: Structures of **TSg** connecting two **ML** minima.

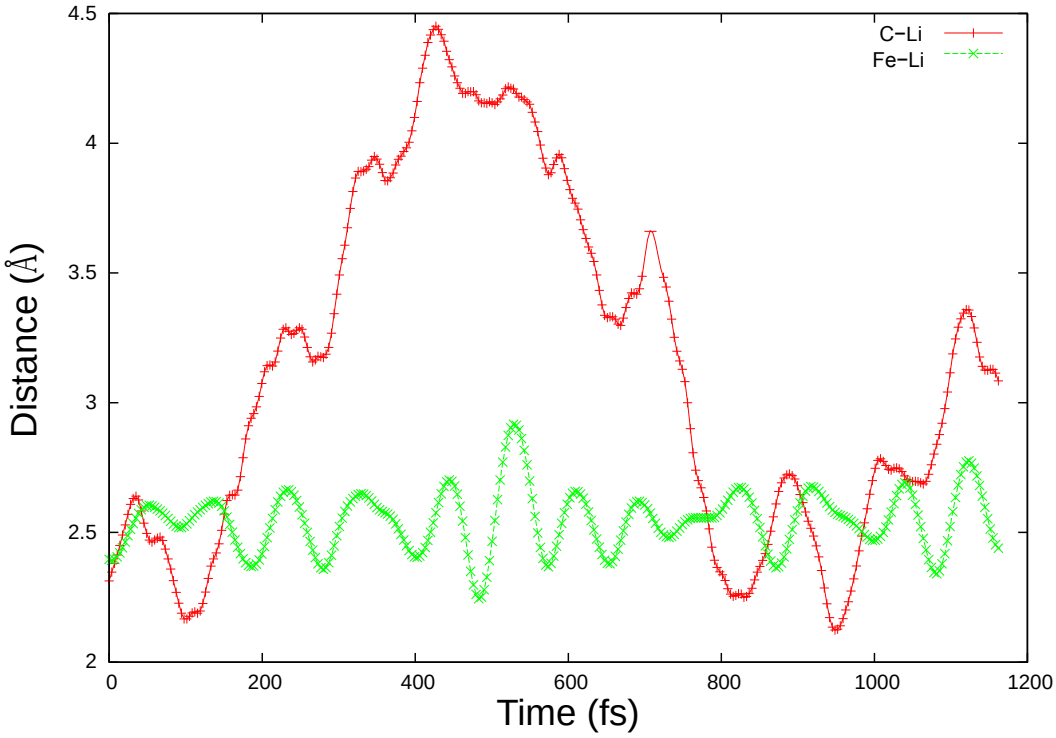

Fig. S8: Fe-Li and C-Li distance as a function of time for a representative trajectory that shows planetary motion.

References

(S1) Lee, C.; Yang, W.; Parr, R. G. *Phys. Rev. B* **1988**, *37*, 785.

(S2) Becke, A. D. *J. Phys. Chem.* **1993**, *98*, 5648.

(S3) Becke, A. D. *Phys. Rev. A* **1988**, *38*, 3098.

(S4) Perdew, J. P. and Wang, Y. *Phys. Rev. B* **1992**, *45*, 13244..

(S5) Godbout, N.; Salahub, D. R.; Andzelm, J.; Wimmer, E. *Can. J. Chem.* **1992**, *70*, 560.

(S6) Sosa, C.; Andzelm, J.; Elkin, B. C.; Wimmer, E.; Dobbs, K. D.; Dixon, D. A. *J. Phys. Chem.* **1992**, *96*, 6630.

(S7) Frisch, M. J. et al. Gaussian-09 Revision C.01. Gaussian Inc. Wallingford CT 2009.

(S8) Valiev, M.; Bylaska, E.; Govind, N.; Kowalski, K.; Straatsma, T.; Dam, H. V.; Wang, D.; Nieplocha, J.; Apra, E.; Windus, T.; de Jong, W. *Comput. Phys. Commun.* **2010**, *181*, 1477.

(S9) Mayor-López, M. J.; Lüthi, H. P.; Koch, H.; Morgantini, P. Y.; Weber, J. *J. Chem. Phys.* **2000**, *113*, 8009.

(S10) Sun, L.; Hase, W. L. *Reviews in Computational Chemistry*; John Wiley & Sons, Inc., 2003; pp 79–146.

(S11) Lourderaj, U.; Song, K.; Windus, T. L.; Zhuang, Y.; Hase, W. L. *J. Chem. Phys.* **2007**, *126*.

(S12) Lourderaj, U.; Sun, R.; Kohale, S. C.; Barnes, G. L.; de Jong, W. A.; Windus, T. L.; Hase, W. L. *Comput. Phys. Commun.* **2014**, *185*, 1074.

(S13) Peslherbe, G. H.; Wang, H.; Hase, W. L. *Advances in Chemical Physics*; John Wiley & Sons, Inc., 2007; pp 171–201.

(S14) Levesque, D.; Verlet, L. *J. Stat. Phys.* **1993**, *72*, 519.